Shear Thinning and Nonlinear Structural Deformation of Ionic Liquids with Long Alkyl Chain Studied by Molecular Dynamics Simulation

Journal:	*The Journal of Physical Chemistry*
Manuscript ID	jp-2019-035577.R1
Manuscript Type:	Article
Date Submitted by the Author:	n/a
Complete List of Authors:	Yamaguchi, Tsuyoshi; Nagoya Daigaku Kogakubu Daigakuin Kogaku Kenkyuka, Department of Materials Process Engineering

Shear Thinning and Nonlinear Structural Deformation of Ionic Liquids with Long Alkyl Chain Studied by Molecular Dynamics Simulation

Tsuyoshi Yamaguchi

Graduate School of Engineering, Nagoya University, Furo-cho, Chikusa, Nagoya, Aichi 464-8603, Japan

ABSTRACT

Non-equilibrium molecular dynamics (MD) simulation was performed on imidazolium-based ionic liquids of two different alkyl chain lengths, and shear-rate dependent viscosity was evaluated. Compared with the frequency-dependent linear shear viscosity determined by equilibrium MD simulation, shear thinning occurs at the shear rate several times lower than that predicted by the Cox-Merz rule. The deformation of structure factor was also evaluated as the function of shear rate. The onset of the shear thinning corresponds to that of the nonlinearity in the deformation of the charge-alternation mode in both ionic liquids, which is in harmony with the result of our previous work that the shear relaxation of ionic liquid is mainly coupled to the structural relaxation of the charge-alternation mode. In the presence of the polar-nonpolar domain structure characteristic to ionic liquids with a long alkyl chain, in particular, the nonlinearity in the domain mode begins within the Newtonian regime of shear viscosity.

1. Introduction

Room-temperature ionic liquid (RTIL) is a class of liquid materials that have been studied intensively for more than a decade. Although RTIL is composed solely of ions, it behaves as a liquid even near the room temperature. Due to peculiar properties of RTIL such as high ionic conductivity, high thermal and electrochemical stabilities, and low vapor pressure, it has found many applications such as electrolytes for electrochemical devices and solvents for organic synthesis.[1,2]

Lubricant is one of the possible applications of RTIL.[3,4,5,6] In elastohydrodynamic lubrication regime where both the pressure and the shear rate at the contact point are high, shear thinning occurs even in RTIL composed of low molecular-weight ions, and the information on the shear thinning is essential to describe lubrication behavior.

Shear viscosity is defined through the response of shear stress to the shear flow. Shear stress originates in the anisotropic deformation of the microscopic structure under shear. It behaves in the Newtonian way when the liquid structure coupled to the shear stress deforms linearly, and the shear thinning is expected when the response of the microscopic structure saturates. Therefore, important points are what structure of liquid is coupled to the shear stress and how it behaves under the shear flow.

In our previous works, we proposed a computational method to extract the coupling between the microscopic structure and the shear stress from equilibrium molecular dynamics (MD) simulation.[7] It was then applied to two imidazolium-based ionic liquids, 1-ethyl-3-methylimidazolium bis(trifluoromethanesulfonyl)amide ([emim][TFSA]) and 1-methyl-3-octylimidazolium TFSA ([omim][TFSA]).[8] The static structure factor of ionic liquids with a long alkyl chain, such as

[omim][TFSA], is known to exhibit a prepeak in low-q region, reflecting the characteristic mesoscopic structure composed of polar and nonpolar domains.[9,10,11] Since the domain structure resembles mesoscopic structure of surfactant solutions that brings about their large structural viscosity, it has been an interesting question how the domain structure of ionic liquids is related to its shear viscosity.[12] Contrary to the expectation, our previous work showed that the coupling between the domain mode and the shear stress in [omim][TFSA] is rather small, and the shear relaxation is dominated by the structural relaxation of the charge-alternation mode in both liquids.[8] However, our previous works are limited to the coupling between the domain structure and the shear stress in the linear regime, and the roles of the domain structure in nonlinear rheology are yet to be resolved.

In this work, we apply non-equilibrium MD simulation to [emim][TFSA] and [omim][TFSA], and evaluate the shear viscosity and the structural deformation under finite shear. In particular, the relation between the nonlinear deformation of the domain structure and the shear thinning of [omim][TFSA] is focused.

2. Computational methods

The systems we consider were two ionic liquids, [emim][TFSA] and [omim][TFSA], which were described by united atom models.[13] In this model, the absolute values of the total charges on an ion are scaled to be $0.8e$, where e stands for the charge of a proton, in order to compensate the retardation of the dynamics associated with the neglect of the electronic polarization. The sizes of both systems were 1000 ion pairs. The simple shear was applied to the system under NVT

ensemble with periodic boundary condition. The temperature of the systems was 353 K, and the densities were fixed to the values at 1 atm determined in our previous work by means of NPT ensemble MD simulation.[8] For each shear rate, a run of 10 ns length was performed to establish steady state, followed by a production run of 100 ns length. All the simulation runs were performed using GROMACS 2016.4 package.[14] Other parameters of the simulation were the same as the equilibrium MD simulation in our previous work.[8]

3. Results and discussion

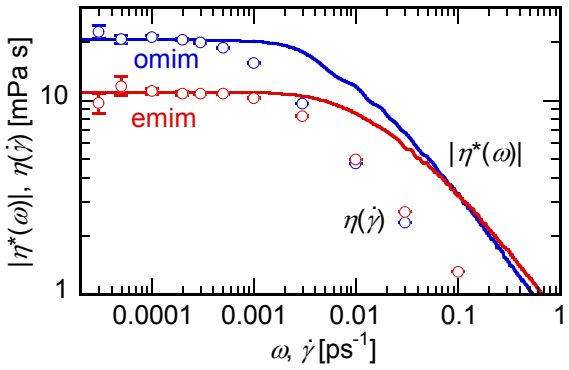

Figure 1. Shear rate dependent shear viscosities (open circles) in this work are compared with the magnitude of the frequency-dependent complex shear viscosities (solid curves). The results of [emim][TFSA] and [omim][TFSA] are plotted with red and blue symbols, respectively.

The simple shear of the shear rate $\dot{\gamma}$ was applied to *xy*-direction, that is, the flow vector is parallel to the *x*-direction and its magnitude linearly depends on *y*, and the statistical average of the *xy*-component of the pressure tensor, $\langle P_{xy} \rangle_{\dot{\gamma}}$, was evaluated, where $\langle \cdots \rangle_{\dot{\gamma}}$ stands for the non-

equilibrium average under shear of the shear rate $\dot{\gamma}$. The shear-rate dependent viscosity, $\eta(\dot{\gamma})$, was defined as

$$\eta(\dot{\gamma}) \equiv \frac{\langle P_{xy} \rangle_{\dot{\gamma}}}{\dot{\gamma}}, \quad (1)$$

and calculated as the function of $\dot{\gamma}$. The results of both ionic liquids are shown in Fig. 1. Newtonian regimes are observed around $\dot{\gamma}$ = 10^{-4} ps^{-1}, and shear thinning is observed at higher shear rates. Comparing [emim][TFSA] and [omim][TFSA], the Newtonian viscosity of the former is lower, and the onset shear rate of the shear thinning of the former is higher than that of the latter.

The frequency-dependent complex shear viscosity, $\eta^*(\omega)$, is related to the equilibrium time correlation function of P_{xy} as

$$\eta^*(\omega) = \frac{V}{k_B T} \int_0^\infty dt\, e^{i\omega t} \langle P_{xy}(t=0) P_{xy}(t) \rangle_{eq}, \quad (2)$$

where ω, k_B, T, and V are angular frequency, Boltzmann constant, absolute temperature and the volume of the system, respectively, and $<\ldots>_{eq}$ denotes the equilibrium ensemble average. The zero-frequency limiting value of $\eta^*(\omega)$ in principle corresponds to the zero-shear limiting value of $\eta(\dot{\gamma})$, denoted as η_0. In this work, $\eta^*(\omega)$ of the two liquids are calculated from the time correlation function $\langle P_{xy}(t=0) P_{xy}(t) \rangle_{eq}$ obtained in the equilibrium MD simulation of our previous work.[8]

Cox-Merz rule is an empirical rule that relates $\eta^*(\omega)$ and $\eta(\dot{\gamma})$ as[15]

$$\eta(\dot{\gamma}) = |\eta^*(\omega)| \text{ at } \dot{\gamma} = \omega. \quad (3)$$

It was originally proposed on polymer melts and solutions, and it works well on these systems. In Fig. 1, we plot $|\eta^*(\omega)|$ of both liquids together with $\eta(\dot{\gamma})$ based on Cox-Merz rule. The horizontal axes are ω and $\dot{\gamma}$ for the former and the latter, respectively, so that they agree with each other when Cox-Merz rule holds.

In both liquids, the low-frequency limiting values of $|\eta^*(\omega)|$ are equal to $\eta(\dot{\gamma})$ in the Newtonian regime, which indicates that the values of η_0 obtained by both equilibrium and non-equilibrium MD simulations are consistent with each other. The onset shear rate of the shear thinning is several times lower than that predicted by $|\eta^*(\omega)|$, which means the breakdown of Cox-Merz rule in these two ionic liquids.

Comparing frequency-dependent linear viscosities, $|\eta^*(\omega)|$, of [emim][TFSA] and [omim][TFSA] at fixed angular frequency, although $|\eta^*(\omega)|$ of the former is smaller than that of the latter at $\omega < 0.1$ ps^{-1}, the relation is inverted at higher ω. The higher $|\eta^*(\omega)|$ in the high-frequency region means the larger plateau modulus of [emim][TFSA], which is ascribed to the larger ionic density.[16,17] The similar inversion is also observed in $\eta(\dot{\gamma})$ at $\dot{\gamma} > 0.01$ ps^{-1}, which suggests that the viscosity under high-shear rate reflects the strength of the instantaneous intermolecular interaction rather than the relaxation dynamics of microscopic structures.

In recent works, we examined the validity of Cox-Merz rule in two representative low molecular-weight liquids as the Lennard-Jones (LJ) liquid[18] and liquid *n*-hexane.[19] The latter follows Cox-Merz rule whereas the former does not. The difference in the validity of Cox-Merz rule in these liquids was ascribed to the difference in the microscopic structure that governs the slowest viscoelastic relaxation. The shear relaxation in LJ liquid was assigned to the anisotropic shift of the peak of the static structure factor, while that of liquid *n*-hexane was to the translation-orientation coupling. Due to the sharp shape of the peak of the static structure factor, small amount of the peak shift results in the deviation of the liquid structure from the equilibrium one, leading to the strong nonlinearity in the shear stress. On the other hand, the distribution of molecular orientation is broad, and its deviation from the equilibrium one requires high shear rate.

We also studied the coupling between the microscopic structure and shear stress of [emim][TFSA] and [omim][TFSA] by means of the cross-correlation analysis of equilibrium MD simulation.[8] The analysis showed that the principal part of the shear viscosity of both ionic liquids originates from the coupling with the charge-density mode. The charge-density modes of both ionic liquids show sharply-peaked structure around 8 nm^{-1}, which suggests the strong nonlinearity of their deformation under shear. We hereafter examine the structure factors of both ionic liquids under shear from our present non-equilibrium MD simulation.

The $\mu\nu$-part of the static structure factor under shear, $\chi_{\mu\nu}^{(ne)}(\mathbf{q};\dot{\gamma})$, is defined as

$$\chi_{\mu\nu}^{(ne)}(\mathbf{q};\dot{\gamma}) \equiv \frac{1}{V}\left\langle \rho_{\mu}^{*}(\mathbf{q})\rho_{\nu}(\mathbf{q})\right\rangle_{\dot{\gamma}}, \tag{4}$$

where μ and ν are indexes for the groups of interaction sites, and the asterisk here indicates the complex conjugate. The weighted number density of μ, denoted as $\rho_{\mu}(\mathbf{q})$, is given by

$$\rho_{\mu}(\mathbf{q}) \equiv \sum_{j\in\mu} b_j e^{i\mathbf{q}\cdot\mathbf{r}_j}, \tag{5}$$

where b_j and $\mathbf{r}_j$ stand for the weighting factor and the position of the site j, respectively. In this work, we employ as b_j the X-ray scattering length in the low-q limit, which is proportional to the number of electrons on the site j.

Although the equilibrium static structure factor, $\chi_{\mu\nu}^{(eq)}(q) \equiv \chi_{\mu\nu}^{(ne)}(|\mathbf{q}|;\dot{\gamma}=0)$, is isotropic, that is, independent of the direction of the vector $\mathbf{q}$, it becomes anisotropic under shear flow. The orientational dependence of $\chi_{\mu\nu}^{(ne)}(\mathbf{q};\dot{\gamma})$ can be expanded over the spherical harmonics as

$$\chi_{\mu\nu}^{(ne)}(\mathbf{q};\dot{\gamma}) = \chi_{iso,\mu\nu}^{(ne)}(q;\dot{\gamma}) + \frac{q_x q_y}{q^2}\chi_{xy,\mu\nu}^{(ne)}(q;\dot{\gamma}) + O(\dot{\gamma}^2), \tag{6}$$

where $q = |\mathbf{q}|$. The isotropic part, $\chi_{iso,\mu\nu}^{(ne)}(q;\dot{\gamma})$, is equal to $\chi_{\mu\nu}^{(eq)}(q)$ in the low-shear limit, and the deviation from the equilibrium structure is $O(\dot{\gamma}^2)$. The xy-component, $\chi_{xy,\mu\nu}^{(ne)}(q;\dot{\gamma})$, is proportional to $\dot{\gamma}$ in the low-shear limit, and other anisotropic components behave in nonlinear ways.

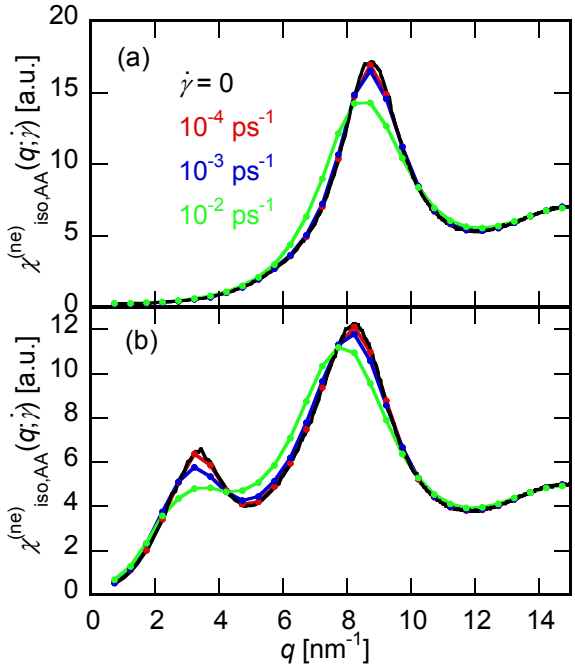

Figure 2. The isotropic components of the anion-anion part of the structure factors, $\chi^{(ne)}_{iso,AA}(q;\dot{\gamma})$, of (a) [emim][TFSA] and (b) [omim][TFSA]. The values of the shear rate are 10^{-4} ps^{-1} (red), 10^{-3} ps^{-1} (blue) and 10^{-2} ps^{-1} (green), respectively. The equilibrium static structure factors, $\chi^{(eq)}_{AA}(q)$, taken from Ref. 8 are also plotted with black curves.

The equilibrium static structure factor, determined in our previous work,[8] is plotted in Fig. 2. Only the anion-anion part, $\chi^{(eq)}_{AA}(q)$, is shown here. A strong peak is observed around q = 8 nm^{-1} in both ionic liquids, which is assigned to the charge-density mode, that is, the cation-anion charge alternating structure. In addition, a prepeak is observed at q = 3 nm^{-1} in the case of [omim][TFSA], which reflects the characteristic intermediate-range structure composed of polar and nonpolar domains. The charge-alternation mode is characterized by the strongly negative cross-correlation between the cationic and anionic groups accompanied with their positive self-correlations.[20,21] On the other hand, both the self- and cross-correlations of both ionic groups are positive at the prepeak.

Therefore, the anion-anion part of the structure factor is positive at both the charge-density mode and the prepeak.

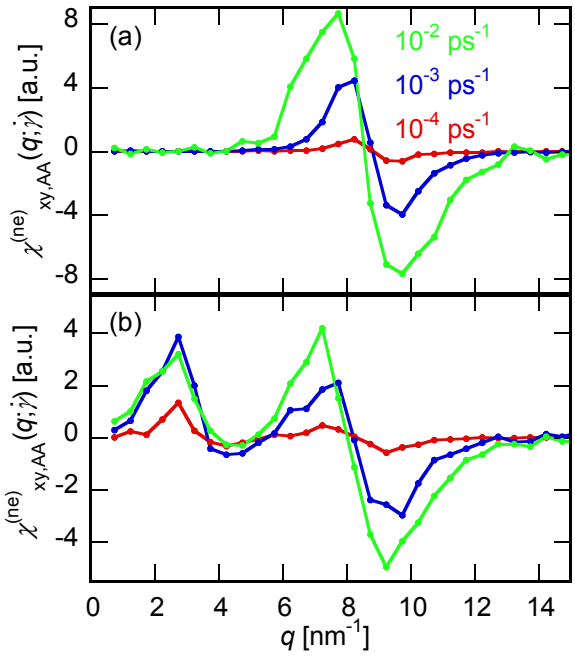

Figure 3. The *xy*-components of the anion-anion part of the structure factors, $\chi^{(ne)}_{xy,AA}(q;\dot{\gamma})$, of (a) [emim][TFSA] and (b) [omim][TFSA]. The values of the shear rate are 10^{-4} ps^{-1} (red), 10^{-3} ps^{-1} (blue) and 10^{-2} ps^{-1} (green), respectively.

The *xy*-components of the structure factor under shear, $\chi^{(ne)}_{xy,AA}(q;\dot{\gamma})$, at three different shear rates are plotted in Fig. 3. In both ionic liquids, derivative-shaped structure is observed at the peak of the static structure factor, 8 nm^{-1}. It indicates the anisotropic shift of the charge-density mode, that is, the peak shifts to lower-q along the extension axis of the shear deformation while it shifts to higher-q along the compression axis. In the case of [omim][TFSA], a strong positive peak at 2.5 nm^{-1} and a weak basin at 4 nm^{-1} are also observed, which means that the prepeak of [omim][TFSA] also shifts in the anisotropic way.

The structural deformation increases with increasing the shear rate. It is theoretically expected to behave linearly in the limit of $\dot{\gamma}\to 0$. Considering that the variation of the shear rate is of the two orders of magnitude in Fig. 3, however, the increase in the structural deformation is much smaller than the expectation of the linear response. Provided that the highest shear rate in Fig. 3, 10^{-2} ps^{-1}, is within the shear thinning regime of the shear stress in both ionic liquids as is demonstrated in Fig. 1, the nonlinearity in the structural deformation in Fig. 3 is consistent with that in the shear stress.

The nonlinearity in the structural deformation is also observed in $\chi^{(ne)}_{iso,AA}(q;\dot{\gamma})$ shown in Fig. 2. Since its variation is proportional to $\dot{\gamma}^2$ in the low-shear limit, its deviation from the equilibrium one, $\chi^{(eq)}_{AA}(q)$, indicates the nonlinear deformation. In both liquids, $\chi^{(ne)}_{iso,AA}(q;\dot{\gamma})$ almost agrees with $\chi^{(eq)}_{AA}(q)$ at $\dot{\gamma}$ = 10^{-4} ps^{-1} where $\eta(\dot{\gamma})$ behaves in the Newtonian way in Fig. 1. The broadening and the decrease in the peak height are observed in both liquids at both peaks in the shear thinning regime, as was reported on the main peak of simple atomic liquids.[22]

Comparing [emim][TFSA] and [omim][TFSA] in the same range of the shear rate, the nonlinearity of the deformation of the charge-density mode at 8 nm^{-1} is stronger in the latter, which is clearly observed by comparing Figs. 3a and 3b. The stronger nonlinearity of [omim][TFSA] is consistent with its lower onset shear rate shown in Fig. 1.

As is shown in both Figs. 2b and 3b, the nonlinearity in the deformation of the prepeak of [omim][TFSA] is larger than that of the charge-density mode. Neutron quasielastic scattering experiments[23,24] and MD simulation[8] demonstrated that the relaxation of the intermediate scattering function at the prepeak is much slower than that of the charge-density mode. We thus consider that the stronger nonlinearity of the deformation of the prepeak is ascribed to its slower dynamics.

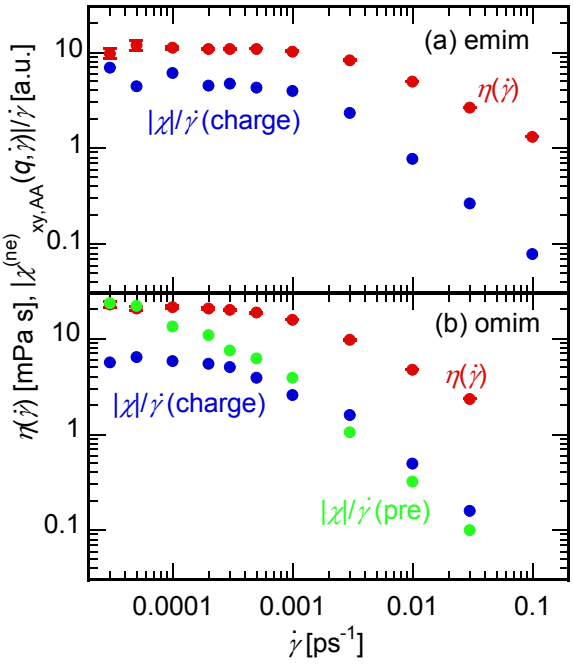

Figure 4. The *xy*-components of the anion-anion part of the structure factors, $\chi^{(ne)}_{xy,AA}(q;\dot{\gamma})$, are divided by the shear rate, $\dot{\gamma}$, and plotted as the functions of the shear rate. The function of [emim][TFSA] averaged over $9.5 < q < 10.0$ nm^{-1} is plotted with blue circles in panel (a), whereas those of [omim][TFSA] averaged over $2.5 < q < 3.0$ nm^{-1} (green) and $9.0 < q < 9.5$ nm^{-1} (blue) are shown in panel (b). The shear-rate dependent viscosities, $\eta(\dot{\gamma})$, of the corresponding liquids are plotted with red circles in both panels for comparison.

The nonlinearity in $\chi^{(ne)}_{xy,AA}(q;\dot{\gamma})$ of the two ionic liquids with respect to $\dot{\gamma}$ is compared with that of the shear stress in Fig. 4. The average of $\chi^{(ne)}_{xy,AA}(q;\dot{\gamma})$ in the q-range of 9.5-10.0 nm^{-1}, corresponding to the position of the negative peak in Fig. 3a, is employed as the measure of the anisotropic shift of the charge-alternation mode of [emim][TFSA]. In the case of [omim][TFSA], the q-ranges of 2.5-3.0 nm^{-1} and 9.0-9.5 nm^{-1} are used for the prepeak and the charge-alternation mode, respectively. $\left|\chi^{(ne)}_{xy,AA}(q;\dot{\gamma})\right|/\dot{\gamma}$ is calculated as the function of $\dot{\gamma}$, and plotted together with $\eta(\dot{\gamma})$ for comparison.

In both liquids, $\left|\chi^{(ne)}_{xy,AA}(q;\dot{\gamma})\right|/\dot{\gamma}$ at the charge-alternation mode, plotted with blue circles, shows a plateau in the low-shear region, and it decreases with $\dot{\gamma}$ at higher shear rate. Compared with $\eta(\dot{\gamma})$, the onset shear rate of the nonlinearity in the deformation of the charge-alternation mode is close to that of the shear thinning. Provided that the deformation of the charge-alternation mode is strongly coupled to the shear stress as was demonstrated in our previous work,[8] the nonlinearity in the shear stress is naturally ascribed to that in the deformation of the charge-alternation mode. The decreases in $\left|\chi^{(ne)}_{xy,AA}(q;\dot{\gamma})\right|/\dot{\gamma}$ of both liquids at the charge-alternation mode is stronger than those of $\eta(\dot{\gamma})$ in the shear-thinning regime. We consider it is ascribed to the contribution of the microscopic structures other than the charge-alternation mode to the shear stress. Although the contribution of the charge-alternation mode decreases proportionally to $\left|\chi^{(ne)}_{xy,AA}(q;\dot{\gamma})\right|/\dot{\gamma}$, the nonlinearity of other modes may be weaker, and its relative contribution to the shear stress can be larger at higher $\dot{\gamma}$, leading to the weaker nonlinearity of the shear stress.

In Fig. 4b, $\left|\chi^{(ne)}_{xy,AA}(q;\dot{\gamma})\right|/\dot{\gamma}$ of [omim][TFSA] at the prepeak is a decreasing function of $\dot{\gamma}$, and the plateau is not observed in the range of $\dot{\gamma}$ studied in this work. In principle, $\chi^{(ne)}_{xy,AA}(q;\dot{\gamma})$ must be proportional to $\dot{\gamma}$ in the low-shear limit, and we consider that the plateau should appear in the range of the shear rate lower than that studied in this work. Although we tried non-equilibrium MD simulation of [omim][TFSA] at lower shear rate, we could not obtain statistically reliable results because the absolute values of both shear stress and the structural deformation are small.

An important point on the deformation of the prepeak of [omim][TFSA] is that the shear stress behaves in the Newtonian way at the shear rate where $\chi^{(ne)}_{xy,AA}(q;\dot{\gamma})$ at the prepeak exhibits nonlinearity. It is in harmony with the result of our previous work that the coupling between the domain structure and the shear stress is weak.[8] The nonlinearity in the deformation of the prepeak hardly appear in $\eta(\dot{\gamma})$ because of the weak coupling. Since the coupling is weak but non-zero,

weak shear thinning may be present at $\dot{\gamma} < 10^{-4}$ ps^{-1}, although we could not detect it within the statistical uncertainty of our MD simulation.

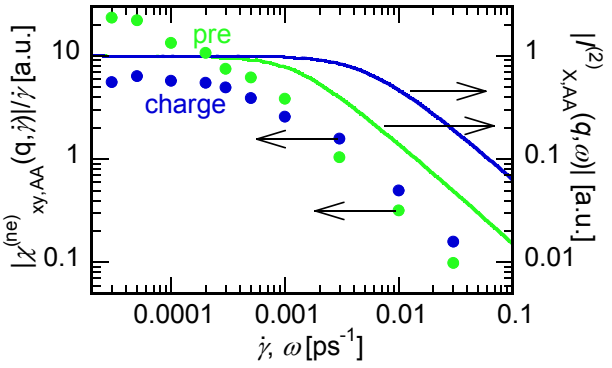

Figure 5. The *xy*-components of the anion-anion part of the structure factors, $\chi^{(ne)}_{xy,AA}(q;\dot{\gamma})$, of [omim][TFSA] divided by the shear rate, $\dot{\gamma}$, (filled circles) are compared with the spectra of the square of intermediate scattering functions, $\left|I^{(2)}_{AA}(q,\omega)\right|$ (solid curves). The formers are averaged over $2.5 < q < 3.0$ nm^{-1} (green) and $9.0 < q < 9.5$ nm^{-1} (blue), whereas the latter functions are plotted at the peaks of both modes, $q = 3.7$ nm^{-1} (green) and 8.1 nm^{-1} (blue), respectively. Both the blue and the green circles are identical to those in Fig. 4b.

The nonlinear response of the anisotropic parts of the structure factor of [omim][TFSA] at two modes is compared with the dynamics of the intermediate scattering function in Fig. 5. Since the equilibrium dynamics of the two-body density mode is proportional to the square of the intermediate scattering function under the factorization approximation,[8] the comparison was performed with the spectrum of the square of the intermediate scattering function defined as

$$I^{(2)}_{X,AA}(q,\omega) \equiv \int_0^\infty dt\, e^{-i\omega t}\left[\frac{1}{V}\left\langle \rho_A^*(\mathbf{q},t=0)\rho_A(\mathbf{q},t)\right\rangle_{eq}\right]^2. \quad (7)$$

The absolute value of $I^{(2)}_{X,AA}(q,\omega)$ was used in Fig. 5 based on the idea of the Cox-Merz rule. The values at two wavenumbers, $q = 3.7$ nm^{-1} and 8.1 nm^{-1}, are chosen as the peak tops of the domain

mode and the charge-density mode, respectively. The intermediate scattering functions are taken from our previous work.[8] As is demonstrated in Fig. 5, the nonlinearity of the response of both modes are stronger than that predicted from the equilibrium structural relaxation at the corresponding modes.

Our theoretical work by means of interaction-site based mode-coupling theory demonstrated that the presence of the domain structure increases the shear viscosity of ionic liquids in two different ways.[25] The first one is the direct coupling, which is shown to be small in the present model of [omim][TFSA]. The second one is that the domain dynamics is coupled to the structural relaxation at the charge-alternation mode in a nonlinear way, which leads to the increase in the shear viscosity through the retardation of the dynamics of the charge-alternation mode. Although we expected in the beginning of this work that the nonlinear deformation of the domain structure may cause shear thinning through the second indirect mechanism, our present MD simulation shows that the effects of such a mechanism are rather weak. We consider it is because the nonlinearity in the isotropic part is small at $\dot{\gamma} < 10^{-4}$ ps^{-1}, as is demonstrated in Fig. 2b.

Cosby and coworkers experimentally demonstrated the presence of a weak and slow relaxation mode in linear viscoelasticity of some ionic liquids that was assigned to the relaxation of the domain mode.[26] The existence of the domain mode had already been predicted by our mode-coupling theoretical calculation,[25] although it was not detected in our equilibrium MD simulation within the statistical relevance.[8] We thus expect that weak shear thinning associated with the nonlinear deformation of the domain structure may be detected by precise measurement of the shear-rate dependent viscosity.

The structure factor under shear, $\chi_{\mu\nu}^{(ne)}(\mathbf{q};\dot{\gamma})$, can be determined experimentally by measuring small-angle X-ray or neutron scattering (abbreviated as “SAXS” or “SANS”, respectively) of a

sample under shear. Such measurements, called "Rheo-SAXS" or "Rheo-SANS",[27] have been applied to rheology of soft materials such as colloidal solutions, polymers, and surfactant systems. The *xy*-component, $\chi^{(ne)}_{xy,\mu\nu}(\mathbf{q};\dot{\gamma})$, is accessible by the irradiation of the incident beam in parallel to the rotational axis in the case of Taylor-Couette flow, for instance. The shear thinning can also be measured using conventional viscometer. Our present work suggests that the comparison between $\chi^{(ne)}_{xy,\mu\nu}(\mathbf{q};\dot{\gamma})$ and $\eta(\dot{\gamma})$ will give us information on the microscopic structure that governs shear viscosity.

4. Summary

The shear-rate dependent viscosity and structural deformation of two ionic liquids, [emim][TFSA] and [omim][TFSA], were evaluated by means of non-equilibrium MD simulation as the functions of the shear rate. The transition between Newtonian and shear-thinning regimes was observed in both ionic liquids. Compared with the frequency-dependent linear complex viscosity, the onset shear rate of the shear thinning was several times lower than the prediction of the Cox-Merz rule.

The deformation of the structure factor under shear was determined as the function of the shear rate. The onset of the nonlinearity in the anisotropic shift of the charge-alternation mode corresponded to that of the shear thinning in both ionic liquids, which was in harmony with our previous equilibrium MD simulation that demonstrated the strong coupling between the charge-alternation mode and the shear stress. The nonlinearity in the deformation of the domain structure was scarcely reflected in the shear thinning, because its coupling with the shear stress was weak.

AUTHOR INFORMATION

Corresponding Author

E-mail to Tsuyoshi Yamaguchi: yamaguchi.tsuyoshi@material.nagoya-u.ac.jp

ACKNOWLEDGMENT

This work was partly supported by the Japan Society for the Promotion of Science (JSPS), KAKENHI Grant-in-Aid for Scientific Research (C) (No. 16K05514). All the MD simulation runs in this work were performed using Research Center for Computational Science, Okazaki, Japan.

References

(1) Armand, M.; Endres, F.; MacFarlene, D.; Ohno, H.; Scrosati, B. Ionic-Liquid Materials for the Electrochemical Challenges of the Future, *Nature Mater.* **2009**, *8*, 621–629.

(2) Hallett, J. P.; Welton, T. Room-Temperature Ionic Liquids: Solvents for Synthesis and Catalysis. 2. *Chem. Rev.* **2011**, *111*, 3508–3576.

(3) Zhou, F.; Liang, Y.; Liu, W. Ionic Liquid Lubricants: Designed Chemistry for Engineering Applications. *Chem. Soc. Rev.* **2009**, *38*, 2590–2599.

(4) Somers, A. E.; Howlett, P. C.; MacFarlane, D. R.; Forsyth, M. A Review of Ionic Liquid Lubricants. *Lubricants* **2013**, *1*, 3–21.

(5) Voeltzel, N.; Vergne, P.; Fillot, N.; Bouscharain, N.; Joly, L. Rheology of an Ionic Liquid with Variable Carreau Exponent: A Full Picture by Molecular Simulation with Experimental Contribution. *Tribol. Lett.* **2016**, *64*, 25.

(6) Voeltzel, N.; Fillot, N.; Vergne, P.; Joly, L. Orders of Magnitude Changes in the Friction of an Ionic Liquid on Carbonaceous Surfaces. *J. Phys. Chem. C* **2018**, *122*, 2145–2154.

(7) Yamaguchi, T.; Faraone, A. Analysis of Shear Viscosity and Viscoelastic Relaxation of Liquid Methanol Based on Molecular Dynamics Simulation and Mode-Coupling Theory. *J. Chem. Phys.* **2017**, *146*, 244506.

(8) Yamaguchi, T. Coupling between Mesoscopic Dynamics and Shear Stress of Room-Temperature Ionic Liquid. *Phys. Chem. Chem. Phys.* **2018**, *20*, 17809–17817.

(9) Canongia Lopes, J. N. A.; Pádua, A. A.; Nanostructural Organization in Ionic Liquids. *J. Phys. Chem. B* **2006**, *110*, 3330–3335.

(10) Triolo, A.; Russina, O.; Bleif, H.-J.; di Cola, E. Nanoscale Segregation in Room Temperature Ionic Liquids. *J. Phys. Chem. B* **2007**, *111*, 4641–4644.

(11) Russina, O.; Triolo, A. New Experimental Evidence Supporting the Mesoscopic Segregation Model in Room Temperature Ionic Liquids. *Faraday Discuss.* **2012**, *154*, 97–109.

(12) Rocha, M. A. A.; Neves, C. M. S. S.; Freire, M. G.; Russina, O.; Triolo, A.; Coutinho, J. A. P.; Santos, L. M. B. F. Alkylimidazolium Based Ionic Liquids; Impact on Cation Symmetry on Their Nanoscale Structural Organization. *J. Phys. Chem. B* **2013**, *117*, 10889–10897.

(13) Zhong, X.; Liu, Z.; Cao, D. Improved Classical United-Atom Force Field for Imidazolium-Based Ionic Liquids: Tetrafluoroborate, Hexafluorophosphate, Methylsulfate, Trifluoromethylsulfonate, Acetate, Trifluoroacetate, and Bis(trifluoromethylsulfonyl)amide. *J. Phys. Chem. B* **2011**, *115*, 10027–10040.

(14) Abraham, M. J.; Murtola, T.; Schulz, R.; Páll, S.; Smith, J. C.; Hess, B.; Lindahl, E. GROMACS: High Performance Molecular Simulations through Multi-Level Parallelism from Laptops to Supercomputers. *SoftwareX*, **2015**, *1–2*, 19–25.

(15) Cox, W. P.; Merz, E. H. Correlation of Dynamic and Steady Flow Viscosities. *J. Polym. Sci.* **1958**, *28*, 619–622.

(16) Yamaguchi, T.; Miyake, S.; Koda, S. Shear Relaxation of Imidazolium-Based Room-Temperature Ionic Liquids. *J. Phys. Chem. B* **2010**, *114*, 8126–8133.

(17) Yamaguchi, T.; Nakahara, E.; Sueda, K.; Koda, S. Interpretation of the Variation of Walden Product of Ionic Liquids with Different Alkyl Chain Lengths in Terms of Relaxation Spectra. *J. Phys. Chem. B* **2013**, *117*, 4121–4126.

(18) Yamaguchi, T. Stress-Structure Coupling and Nonlinear Rheology of Lennard-Jones liquid. *J. Chem. Phys.* **2018**, *148*, 234507.

(19) Yamaguchi, T.; Matsuoka, T. Translation-Orientation Coupling and Cox-Merz Rule of Liquid Hexane, *J. Chem. Phys.* **2018**, *149*, 204502.

(20) Kashyap, H. K.; Hettige, J. J.; Annapureddy, H. V. R.; Margulis, C. J. SAXS Anti-Peaks Reveal the Length-Scales of Dual Positive-Negative and Polar-Apolar Ordering in Room-Temperature Ionic Liquids. *Chem. Commun.* **2012**, *48*, 5103–5105.

(21) Perera, A.; Mazighi, R. Simple and Complex Forms of Disorder in Ionic Liquids. *J. Mol. Liq.* **2015**, *210*, 243–251.

(22) Miyazaki K.; Reighman, D. R.; Yamamoto, R. Supercooled Liquids under Shear: Theory and Simulation. *Phys. Rev. E* **2004**, *70*, 011501.

(23) Yamamuro, O.; Yamada, T.; Kofu, M.; Nakakoshi, M.; Nagao, M. Hierarchical Structure and Dynamics of an Ionic Liquid 1-Octyl-3-methylimidazolium Chloride. *J. Chem. Phys.* **2011**, *135*, 054508.

(24) Kofu, M.; Nagao, M.; Ueki, T.; Kitazawa, Y.; Nakamura, Y.; Sawamura, S.; Watanabe, M.; Yamamuro, O. Heterogeneous Slow Dynamics of Imidazolium-Based Ionic Liquids Studied by Neutron Spin Echo. *J. Phys. Chem. B* **2013**, *117*, 2773–2781.

(25) Yamaguchi, T. Mode-Coupling Theoretical Study on the Roles of Heterogeneous Structure in Rheology of Ionic Liquids. *J. Chem. Phys.* **2016**, *144*, 124514.

(26) Cosby, T.; Vicars, Z.; Wang, Y.; Sangoro, J. Dynamic-Mechanical and Dielectric Evidence of Long-Lived Mesoscale Organization in Ionic Liquids. *J. Phys. Chem. Lett.* **2017**, *8*, 3544–3548.

(27) Lindner, P.; Schweins, R.; Campbell, R. A. Sample Environment: Soft Matter Sample Environment for Small-Angle Neutron Scattering and Neutron Reflectometry. In *Neutron in Soft Matter*; Wiley: Hoboken, 2011.

TOC Graphics